ACS APPLIED MATERIALS & INTERFACES

Letter

www.acsami.org

Highly Electrocatalytic $Cu_2ZnSn(S_{1-x}Se_x)_4$ Counter Electrodes for Quantum-Dot-Sensitized Solar Cells

Yuebin Cao,[†] Yanjun Xiao,[†] Jin-Young Jung,[†] Han-Don Um,[†] Sang-Won Jee,[†] Hye Mi Choi,[‡] Jin Ho Bang,*[,‡] and Jung-Ho Lee*[,†]

[†]Department of Chemical Engineering and [‡]Department of Chemistry and Applied Chemistry, Hanyang University, 55 Hanyangdaehak-ro, Sangnok-gu, Ansan, Kyeonggi-do 426-791, Republic of Korea

Supporting Information

ABSTRACT: Traditional Pt counter electrode in quantum-dot-sensitized solar cells suffers from a low electrocatalytic activity and instability due to irreversible surface adsorption of sulfur species incurred while regenerating polysulfide (S_n^{2-}/S^{2-}) electrolytes. To overcome such constraints, chemically synthesized $Cu_2ZnSn(S_{1-x}Se_x)_4$ nanocrystals were evaluated as an alternative to Pt. The resulting chalcogenides exhibited remarkable electrocatalytic activities for reduction of polysulfide (S_n^{2-}) to sulfide (S^{2-}), which were dictated by the ratios of S/Se. In this study, a quantum dot sensitized solar cell constructed with $Cu_2ZnSn(S_{0.5}Se_{0.5})_4$ as a counter electrode showed the highest energy conversion efficiency of 3.01%, which was even higher than that using Pt (1.24%). The compositional variations in between Cu_2ZnSnS_4 ($x = 0$) and $Cu_2ZnSnSe_4$ ($x = 1$) revealed that the solar cell performances were closely related to a difference in electrocatalytic activities for polysulfide reduction governed by the S/Se ratios.

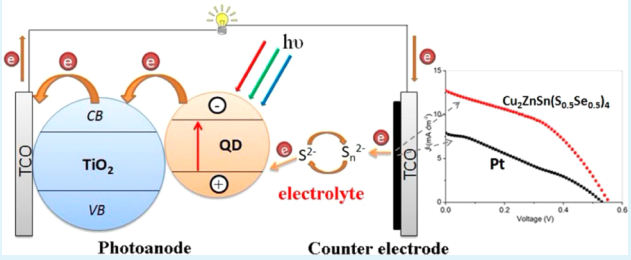

KEYWORDS: *quantum-dot-sensitized solar cells, copper zinc tin sulfur (selenium), counter electrodes, electrocatalytic activity*

1. INTRODUCTION

In principle, quantum-dot-sensitized solar cells (QDSSCs) adopt the design of dye-sensitized solar cells (DSSCs) which are a cost-efficient candidate for next generation solar cells.[1−4] As an alternative to dye molecules of DSSCs, semiconductor quantum dots (QDs) using CdS, CdSe, SnS, Sb_2S_3, or PbS have been employed as sensitizers for QDSSCs.[5−10] The advantages of QDs as photon harvesters include size-dependent bandgap tunability, rapid charge separation,[11] hot electron injection,[12] and multiple exciton generation.[13] A typical configuration of QDSSC devices includes a nanoporous TiO_2 anode sensitized with QDs, an electrolyte containing a redox couple, and a Pt counter electrode (CE). The most efficient electrolyte adopted in DSSCs, I_3^-/I^-, is unfortunately improper for QDSSCs because the majority of QD sensitizers are subjected to severe photodegradation when used in conjunction with the I_3^-/I^- electrolyte.[10] To date, the most optimal electrolyte for QDSSCs is a polysulfide couple (S_n^{2-}/S^{2-}) that can effectively stabilize the QDs while improving the performance of QDSSCs constructed with cadmium chalcogenides as a sensitizer.[14] However, a critical need exists to develop alternative CE materials to replace conventional Pt CE for efficient polysulfide reduction, as the electrocatalytic activity and conductivity of the Pt CE are prone to diminish significantly because of the chemisorption of sulfur compounds, which causes a substantially increased charge transfer resistance at the electrolyte/CE interface.[15]

Recently, various non-platinum-based materials such as Cu_2S,[16,17] CoS,[18] PbS,[19] reduced graphene oxide (RGO)−Cu_2S composite,[20] and hollow carbon,[21,22] have been reported as possible candidates for CE in QDSSCs. In solar cell applications, Cu_2ZnSnS_4 (CZTS) is a promising light absorber that consists of earth-abundant elements while possessing a direct bandgap of ∼1.5 eV with a high absorption coefficient ($>1 \times 10^4$ cm^{-1}).[23−25] Because of these unique properties of CZTS for highly efficient thin-film light harvesters, a large number of studies have reported the development of CZTS-based photovoltaics,[26−28] however few have evaluated cathode applications in solar cells. One interesting study reported that CZTS can be exploited as an effective CE material in DSSCs; moreover, its catalytic activity for I_3^- reduction is comparable to that of Pt CE.[29] Because a few binary metal sulfides, i.e., Cu_2S,[16] CoS,[18] NiS,[18] and PbS,[19] have successfully been utilized as a CE material, the application of multielemental chalcogenides, $Cu_2ZnSn(S,Se)_4$, might also be attractive as a novel electrocatalyst for polysulfide reduction in QDSSC. To explore their possible use, we prepared a series of $Cu_2ZnSn(S_{1-x}Se_x)_4$ (CZTSSe) nanocrystals with different S/Se ratios ($x = 0$, 0.2, 0.5, 0.85, and 1) to investigate their performance as CEs in QDSSCs. We observed the superior electrocatalytic activities of CEs comprised of CZTSSe nanocrystals compared

Received: October 30, 2012
Accepted: January 8, 2013
Published: January 8, 2013

to that of Pt. This feature was found to be closely related to their compositional ratio, i.e., S/Se ratios. In our study, a QDSSC employing $x = 0.5$ showed a high conversion efficiency of 3.01% in contrast to the 1.24% observed with Pt CE. The implication of these results is discussed in attempt to elucidate the mechanism behind this observation.

2. EXPERIMENTAL SECTION

2.1. Synthesis of Cu_2ZnSnS_4 Nanocrystals. In a typical synthesis, copper(II) acetate (1.4 mmol), zinc acetylacetonate (0.96 mmol), tin(IV) acetate (0.8 mmol), and oleylamine (OLA, 12 mL) were mixed and heated under vacuum up to 120 °C to completely dissolve the precursors (OLA-metal-precursors). After degassing at 120 °C for 30 mins, N_2 was purged and the temperature was raised to 230 °C. Subsequently, a solution (OLA-S), in which sulfur powder (S, 6 mmol) was dissolved in OLA (4 mL) *via* sonication, was injected into the OLA-metal-precursors solution. Black CZTS nanocrystals were formed after heating the solution at 230 °C for 30 mins. The mixture was then cooled to room temperature naturally, and an aliquot of methanol (25 mL) was added into the mixture. Next, the nanocrystals were collected by centrifugation. The supernatant was then decanted, and the precipitate was redispersed in toluene (5 mL). The CZTS nanocrystals were finally purified by three alternating precipitations (with methanol) and redispersion (with toluene) cycles as described above.

2.2. Synthesis of $Cu_2ZnSn(S_{1-x}Se_x)_4$ Nanocrystals with $x = 0.2, 0.5, 0.85$, and 1. Unlike sulfur selenium (Se) is insoluble in OLA at ambient temperature, and thus we adapted a different approach for the synthesis of $Cu_2ZnSn(S_{1-x}Se_x)_4$. A desired amount of Se powder was first dissolved in OLA (OLA-Se) at high temperature, and a mixture of OLA-S and OLA-metal-precursors were injected into this solution. Typically, 0.4, 0.55, 0.72, or 0.8 mmol of Se powder was added into OLA (18 mL) and heated at 250 °C under N_2 for ∼1 h to form OLA-Se solution with different Se concentrations. The temperature of OLA-Se solution was then decreased to 240 °C and held at this temperature until injection. OLA-S solutions with different concentrations were prepared by sonication of S powders (0.4, 0.25, 0.08, or 0 mmol) in OLA (3 mL). For the preparation of OLA-metal-precursors solution, copper(II) acetate (0.175 mmol), zinc acetylacetonate (0.12 mmol), tin(IV) acetate (0.1 mmol), and OLA (3 mL) were mixed, heated under vacuum to 120 °C, and degassed for 30 mins to remove traces of water. The solution was then naturally cooled to ambient temperature under N_2 flow. OLA-S solutions were first injected into the OLA-Se solution at 240 °C, and the injection of OLA-metal-precursors followed 5 s after the first injection. CZTSSe nanocrystals formed when the solution was heated at 240 °C for additional 30 min. Finally, the CZTSSe nanocrystals were purified according to the purification procedures used for CZTS nanocrystals.

2.3. Preparation of CZTSSe ($x = 0, 0.2, 0.5, 0.85$, and 1) and Pt CEs. Prior to film fabrication, CZTSSe nanocrystal inks were prepared via the following ligand exchange procedure: the OLA-capped CZTSSe nanocrystals were dispersed in hexanethiol/toluene (volume ratio = 1:10) solution and refluxed at 50 °C for 3 h. The CZTSSe nanocrystals coated with hexanethiol were then dispersed in toluene. For the preparation of CZTSSe CEs, F-doped tin oxide (FTO) substrates (1 × 5 cm) were first cleaned thoroughly by sonication in acetone, ethanol, and deionized water for 30 mins, sequentially. The CZTSSe nanocrystal inks were deposited onto the FTO glass by drop-casting to form nanocrystal thin films, which were then annealed under an Ar flow at 350 °C for 40 mins. Pt-coated FTO glass was prepared by sputtering method.

2.4. Preparation of Photoanodes and Cell Fabrication. Photoanodes (TiO_2/CdS/CdSe/ZnS) for QDSSCs were prepared according to a previous report with some modification.[7] Briefly, TiO_2 paste composed of P25 (Evonik Industries) was spin-coated onto FTO glass and sintered at 450 °C for 30 mins. The spin coating was performed twice to ensure a TiO_2 film thickness of ∼10 μm. QDs were deposited onto the TiO_2 photoelectrode through successive ionic layer adsorption and reaction (SILAR) process. For CdS QDs deposition, the TiO_2 film was dipped into an ethanolic solution of $Cd(NO_3)_2$ (0.5 M) for 5 mins, rinsed with ethanol, dipped for another 5 mins into a methanolic solution of Na_2S (0.5 M), and then rinsed again with methanol. This sequential coating of CdS QDs was repeated three times. For CdSe QDs deposition, sodium selenosulphate (Na_2SeSO_3) was used as a Se source for SILAR. The aqueous Na_2SeSO_3 solution was prepared by refluxing Se (0.3 M) in an aqueous Na_2SO_3 solution (0.6 M) at 70 °C for 7 h. The SILAR process for CdSe deposition was similar to that for CdS except that a longer time (1 h) and higher temperature (50 °C) were used when dipping the film into the Na_2SeSO_3 solution. The sequential coating for CdSe QDs was repeated four times. Finally, a ZnS passivation layer was deposited by dipping the TiO_2/CdS/CdSe film alternatively into aqueous $Zn(CH_3COO)_2$ (0.1 M) and Na_2S (0.1 M) solutions for 1 min twice. Next, the QD sensitized TiO_2 photoanodes and CZTSSe or Pt CEs were assembled into sandwich-type cells, after which a polysulfide solution containing Na_2S (0.5 M), S (0.125 M), and KCl (0.2 M) in water/methanol (volume ratio 7:3) was employed as an electrolyte.

2.5. Characterization. The crystalline phase of CZTSSe nanocrystals was examined with a X-ray diffractometer (X'Pert PRO, PANalytical, Cu Kα radiation) operated at 40 kV and 30 mA. The size and morphology of CZTSSe nanocrystals were analyzed with a transmission electron microscope (TEM, JEOL JEM-2010) at an acceleration voltage of 200 kV. The thickness and morphology of thin CZTSSe films were characterized using a field-emission scanning electron microscope (FESEM, Hitachi S-4800). Current-Voltage ($I-V$) of QDSSCs were measured under the illumination of an AM 1.5G (100 mW/cm^2) using a solar simulator (Peccel PEC-L11). Electrocatalytic activities of CZTSSe nanocrystals were investigated using electrochemical impendence spectroscopy combined with linear sweep voltammetry. Linear sweep voltammetry (LSV) was performed with an electrochemical station (IviumStat) under a three-electrode system, where either CZTSSe/FTO or Pt/FTO served as the working electrode, Pt served as the counter electrode, and Ag/AgCl was used as a reference electrode at a scan rate of 20 mV/s. The electrolyte used for LSV was a N_2-purged water/methanol (volume ratio 7:3) solution containing Na_2S (0.02 M), S (0.02 M), and KCl (0.2 M) as a supporting electrolyte. For electrochemical impendence spectroscopy (EIS) measurement, symmetrical cells were prepared by assembling two identical CZTSSe CEs (or Pt CEs) face-to-face and filling the polysulfide electrolyte in a manner similar to that used for the fabrication of QDSSCs. EIS were measured using an electrochemical station (IviumStat) with a frequency range of 0.1 Hz to 100 kHz and a perturbation amplitude of 10 mV.

3. RESULTS AND DISCUSSION

The synthesis of $Cu_2ZnSn(S_{1-x}Se_x)_4$ (x = 0, 0.2, 0.5, 0.85, and 1) nanocrystals was carried out using a hot injection method. The composition ratios of Cu:Zn:Sn:S:Se in precursors and nanocrystals were determined by X-ray fluorescence (XRF) analysis and listed in Table S1 in the Supporting Information. Our synthetic route allowed for delicate adjustment of the Se content in CZTSSe nanocrystals such that we were able to prepare CZTSSe nanocrystals with various ratios of Se (x = 0, 0.2, 0.5, 0.85, 1). The X-ray diffraction (XRD) patterns (Figure 1) of the CZTS and CZTSe nanocrystals matched well with the

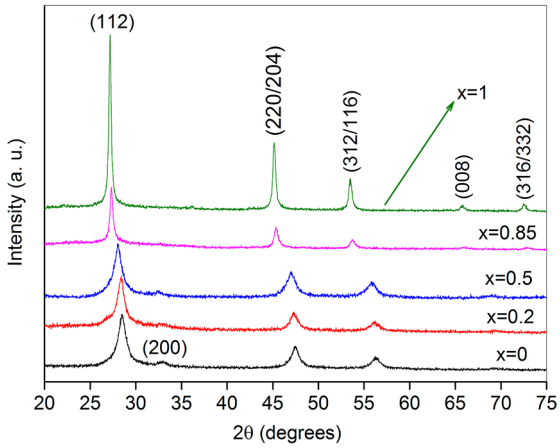

Figure 1. XRD patterns of $Cu_2ZnSn(S_{1-x}Se_x)_4$ nanocrystals synthesized with different S/Se ratios.

tetragonal phases of Cu_2ZnSnS_4 (JCPDS 26-0575) and $Cu_2ZnSnSe_4$ (JCPDS 52-0868), respectively. Tetragonal CZTS and CZTSe phases are normally crystallized in either kesterite ($I\bar{4}$) or stannite ($I\bar{4}2m$) structures. However, it is very difficult to discern kesterite and stannite structures via characterization of XRD patterns because the subtle differences in the degree of tetragonal distortion ($c/2a$) reveal a very weak modulation in the peak splitting of higher-order planes such as (220)/(204) and (116)/(312). Moreover, as frequently reported,[25,30] the peak broadening in XRD patterns prevents the precise classification of CZTSSe crystal structures. Recent first-principle calculations for both CZTS and CZTSe reported that the band configurations of a kesterite structure were more energetically favorable than those of stannite,[31] such that Mitzi and colleagues have described a CZTSSe family as kesterite.[32] In addition, neutron diffractometry results indicate that both CZTS and CZTSe indeed possess a kesterite structure.[33] These previous studies reasonably suggest that the crystal structure of our CZTSSe nanocrystals was mostly based on a kesterite phase. As the Se amount increased, the diffraction peak shifted towards lower angles because the lattice parameters (Table S1 in the Supporting Information) likely expanded with increasing replacement of smaller S atoms (1.84 Å) by larger Se atoms (1.98 Å) in a CZTSSe lattice. Panels a and b in Figure 2 show that the lattice parameters a and c of CZTSSe followed a linear relation with respect to the increase of Se content (Vegard's Law). High-resolution transmission electron microscopy (HRTEM) also supported our XRD results. The interplanar spacing in the CZTS nanocrystal was measured to be ~0.312 nm (Figure 2c), corresponding to (112) planes in the CZTS phase. In accordance with the variation of lattice parameters dictated by Vegard's Law, the interplanar distance increased linearly up to 0.328 nm with increasing Se content (see Figure S2 in the Supporting Information). We also observed that the diffraction peaks became narrower as the amount of Se atoms overall dominated the S in CZTSSe nanocrystals. This implies that the average particle sizes of CZTSSe with higher Se content ($x \geq 0.85$) were larger than those with lower Se content ($x \leq 0.5$), which was clarified from the distribution histograms of particle sizes obtained by analyzing the TEM images (see Figure S1 in the Supporting Information).

Figure 3 shows the SEM images of CZTSSe (x = 0.5) films annealed at 350 °C for 40 min in Ar after drop-casting the

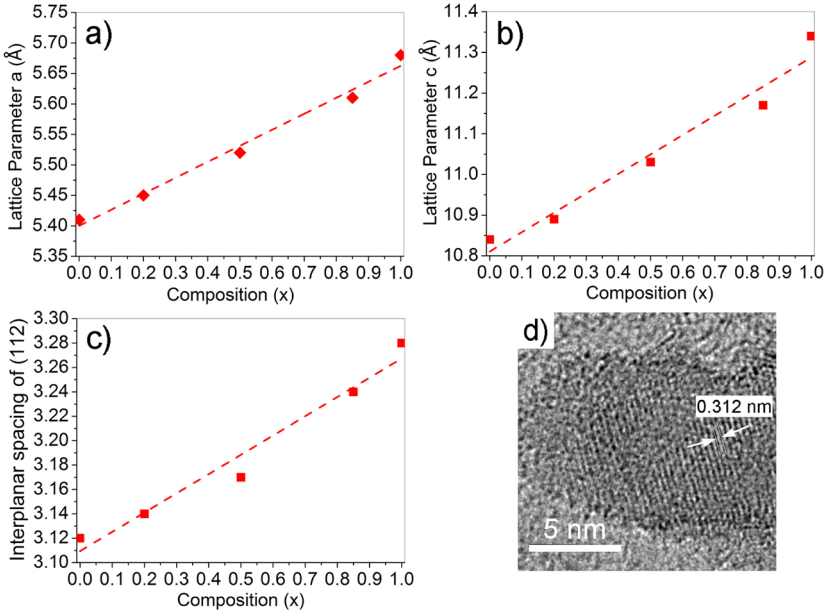

Figure 2. (a–c) Parametric changes in $Cu_2ZnSn(S_{1-x}Se_x)_4$ nanocrystals as a function of x varied from 0 to 1: (a, b) lattice parameters (a, c) determined by XRD; (c) interplanar spacing of (112) determined by HRTEM analysis. All graphs show a linear increment with increasing Se content according to Vegard's Law. (d) HRTEM image of Cu_2ZnSnS_4 nanocrystal; the lattice spacing corresponds to its (112) crystal planes.

dx.doi.org/10.1021/am302522c | ACS Appl. Mater. Interfaces 2013, 5, 479–484

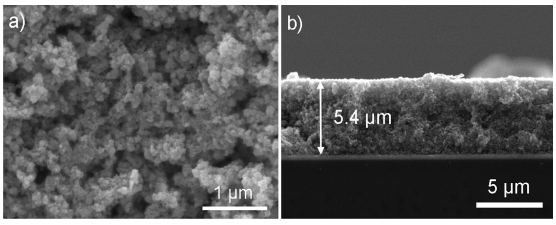

Figure 3. SEM images showing the CZTSSe (x = 0.5) film annealed on a FTO-coated glass; (a) top-view and (b) cross-sectional-view.

CZTSSe inks onto a FTO glass substrate. The nanocrystals normally aggregated to form a porous film (top-view), but the overall film thickness was rather uniform with a thickness of ~5.4 μm (cross-sectional view). The porous structure of CZTSSe films was related with the composition ratios. Specifically, the surfaces of CZTSSe films with low x contents ($x \leq 0.2$) were compact with less porosity (see Figure S3a, b in the Supporting Information). However, with increasing Se content, the surface morphology became porous and loosely packed (see Figure S3c, d in the Supporting Information). The different diffusion rates between S and Se may significantly affect the surface morphology during sintering. One recent study reported that the increased Se content improves the mass transport behavior inside CZTSSe films during annealing.[24]

Regardless of the Se amount, all of the QDSSCs employing CZTSSe as CEs exhibited superior current-voltage characteristics compared to QDSSCs employing Pt CE, as shown in Figure 4 and Table 1. In particular, the QDSSC adopting

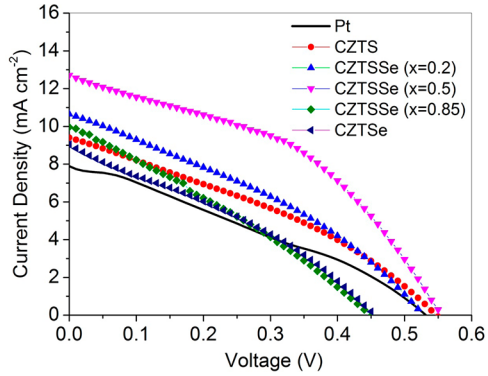

Figure 4. I–V characteristics of QDSSCs fabricated with CEs of CZTSSe and Pt.

CZTSSe of x = 0.5 revealed the highest conversion efficiency (η = 3.01%) owing to a high fill factor (FF) of 0.43 as well as a short-current density (J_{sc}) of 12.71 mA/cm^2. To evaluate the electrocatalytic activities of CZTSSe electrodes for reduction of S_n^{2-}, a linear sweep voltammetry (LSV) was performed in a S_n^{2-}/S^{2-} methanol/water solution containing 0.2 M KCl as a supporting electrolyte (Figure 5a). The CZTSSe (x = 0.5) electrode showed an obvious reduction peak at −0.57 V, ascribed to the reduction of S_n^{2-} into S^{2-} according to eq 1

$$S_n^{2-} + 2e \rightarrow S_{n-1}^{2-} + S^{2-} \quad (1)$$

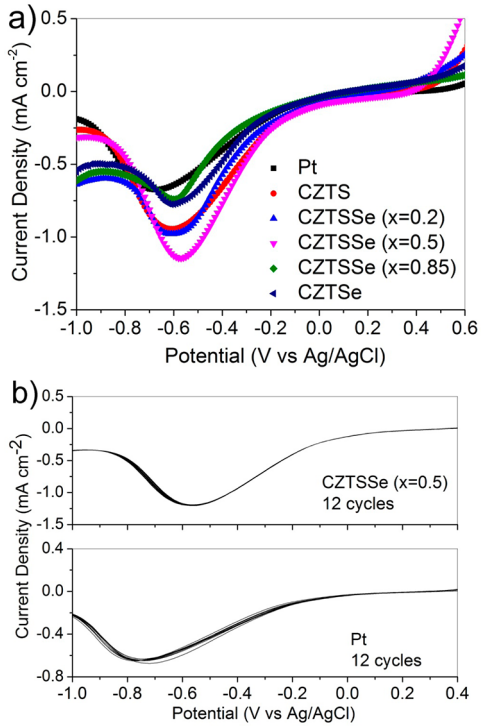

Figure 5. LSV of CEs in 0.02 M/0.02M polysulfide methanol/water solution (volume ratio 3:7) containing 0.2 M KCl as supporting electrolyte: (a) Pt and CZTSSe (x = 0–1) and (b) 12 LSV cycling results of CZTSSe at x = 0.5 (top) and Pt electrode (bottom).

Note that the peak position of CZTSSe (x = 0.5) electrode was found to shift to a rather positive potential side compared to other electrodes, which revealed that the reduction occurred at a lower overpotential. A higher current density of 1.15 mA/cm^2 of the CZTSSe (x = 0.5) electrode also demonstrated the most remarkable electrocatalytic activity out of all the other electrodes. Compared to CZTSSe electrodes with lower Se contents ($x \leq 0.5$), the higher Se content ($x \geq 0.85$) electrodes exhibited lower current densities, explaining their inferior electrocatalytic activity. The Pt electrode showed the most inferior catalytic activity, with the lowest current density and highest overpotential for the S_n^{2-} reduction. The stability of electrodes in the polysulfide electrolyte was investigated by LSV cycling measurement (Figure 5b). No obvious changes in peak potentials and current densities were observed in twelve LSV cycles of a CZTSSe (x = 0.5) electrode, which explained its

Table 1. Photovoltaic Performances of QDDSCs with Different CEs and EIS Parameters of Each CE

counter electrode	J_{sc} (mA cm^{-2})	V_{oc} (V)	FF	η (%)	R_s (Ω)	R_{ct} (Ω)	Z_w (Ω)
CZTS	9.4	0.54	0.339	1.72	16.57	2.59	13.02
CZTSSe (x = 0.2)	10.65	0.52	0.341	1.89	16.71	4.53	3.98
CZTSSe (x = 0.5)	12.71	0.55	0.43	3.01	16.08	1.89	
CZTSSe (x = 0.85)	9.96	0.44	0.299	1.31	15.25	12.8	
CZTSe	9.04	0.45	0.323	1.31	16.02	10.61	
Pt	7.89	0.53	0.295	1.24	10.79	38.5	

dx.doi.org/10.1021/am302522c | ACS Appl. Mater. Interfaces 2013, 5, 479–484

good electrochemical stability in the polysulfide solution. However, the irreversible adsorption of S species onto the Pt surface caused the peak position to shift to a rather negative direction after 12 LSV cycles (Figure 5b, bottom), unveiling the instability of Pt in the polysulfide electrolyte.

To investigate the origin of composition-dependent electrochemical activities, electrochemical impedance spectroscopy (EIS) was performed via symmetrical dummy cells adopting the sandwich structure of counter electrodes and electrolyte, i.e., CE/electrolyte/CE (see Figure S4a in the Supporting Information). Specifically, Nyquist plots were generated from each CE and are shown in Figure 6. All impedance parameters

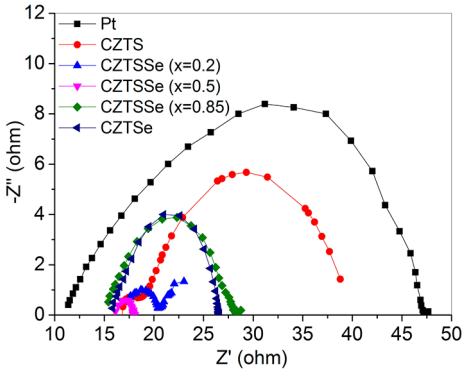

Figure 6. Nyquist plots of Pt and CZTSSe electrodes measured using symmetric cells.

were extracted using Z-VIEW software, from which each Nyquist plot was fitted with an equivalent circuit depicted in Figure S4b in the Supporting Information, where R_s is the ohmic serial resistance, R_{ct} is the charge-transfer resistance, Z_w is the Nernst diffusion impedance of a S_n^{2-}/S^{2-} couple in electrolyte, and CPE is the constant phase angle element at the electrolyte/CE interface. In typical EIS analyses, R_s is normally determined by monitoring the real-axis value at the high-frequency intercept. Previous reports[22,34,35] also denote R_{ct} and Z_w as being derived from semicircles in high- and low-frequency regimes, respectively (a graphic example is shown in Figure S4c in the Supporting Information). The EIS parameters are summarized in Table 1. R_s values in all CZTSSe electrodes were similar, but larger than that of a Pt electrode. Larger R_s values of CZTSSe CEs originated from the poorer conductivities of CZTSSe compared with Pt CE. R_{ct} stands for the electron transfer kinetics at the electrolyte/electrode interface. The much larger R_{ct} value (38.5 Ω) of the Pt CE was indicative of its inferior electron transfer kinetics for S_n^{2-} reduction, which was attributed to the corrosion of a Pt surface by various S species. The best electron transfer kinetics was observed in the CZTSSe CE of x = 0.5, which had the smallest R_{ct} value (1.89 Ω). The CZTS and CZTSSe (x = 0.2) CEs also showed good results with respect to R_{ct}, but suffered from some diffusion resistances (Z_w) that adversely influenced solar cell performances (in accordance with $I-V$ results of Figure 4). The diffusion resistances in these CEs were attributed to their compact surface morphologies, which considerably hindered the diffusion behavior of electrolyte throughout the CEs (see SEM images in Figure S3a and b in the Supporting Information).

From the LSV and EIS results, we found that the electrocatalytic activity of CZTSSe CEs depended critically upon their compositional variations in conjunction with porosities. In this study, CZTS was observed to be intrinsically better than CZTSe for the regeneration of S^{2-} because the R_{ct} of CTZS was much smaller than that of CZTSe. Partial replacement of S in the CZTS by Se slightly changed R_{ct}. R_{ct} became even smaller than that of CTZS when a half of S was replaced with Se. Although no general variation tendency was observed in R_{ct}, our study discovered that R_{ct} varied as a function of Se amounts such that the compositional variations played a crucial role in electrocatalytic activity. Despite the small R_{ct} values of CZTS and CZTSSe (x = 0.2) CEs, their electrocatalytic activities were much less than that of CZTSSe (x = 0.5) CE, implying that the compositional variations have another influence on the electrocatalytic activity. Our EIS study revealed that only CZTS and CZTSSe (x = 0.2) CEs reported Z_w values that were attributed to the compact nature of these CE morphologies (see Table 1 and Figure S3 in the Supporting Information). These surface characteristics hampered the effective diffusion behavior of the electrolytes, leading to the deterioration in electrocatalytic activity. Increasing the Se content in CZTSSe nanocrystals led to the formation of porous films, thus such diffusion impedance no longer exerted the influence on electrocatalytic activity of Se-rich CZTSSe CEs. This argument is supported by the EIS analysis where only charge transfer resistance dictated the electrocatalytic activity when the amount of Se began to be more dominant over S in the composition of CZTSSe. In our current study, 1:1 ratio of S:Se was found to be optimal due to the smallest R_{ct} with no Z_w value, thus the CE made of CZTSSe (x = 0.5) produced the best solar cell performances.

4. CONCLUSIONS

In summary, we demonstrated a new synthetic approach to prepare $Cu_2ZnSn(S_{1-x}Se_x)_4$ nanocrystals with various S/Se ratios (x = 0, 0.2, 0.5, 0.85, and 1). The films fabricated with the CZTSSe nanocrystals exhibited remarkable electrocatalytic performances for regeneration of S^{2-} from S_n^{2-} compared to traditional Pt films. The ratios of S/Se were found to play a crucial role in determining the electrocatalytic activities for S_n^{2-} reduction. LSV and EIS studies also revealed that the electron transfer kinetics and diffusion resistance of electrolyte were dictated by the S/Se ratios. In our study, the QDSSC with CZTSSe (x = 0.5) CE showed the highest energy conversion efficiency of 3.01%, which was higher than that (1.24%) obtained using Pt CE.

■ ASSOCIATED CONTENT

Supporting Information

Compositions and lattice parameters of CZTSSe nanocrystals; relationship of lattice parameters, interplanar distance as a function of CZTSSe composition; TEM images and size distribution histograms of CZTSSe nanocrystals; SEM images of CZTSSe (x = 0, 0.2, 0.85, and 1) CEs; scheme of symmetric cells for EIS measurements; and equivalent circuit model for EIS data fitting. This material is available free of charge via the Internet at http://pubs.acs.org.

■ AUTHOR INFORMATION

Corresponding Author

*E-mail: jungho@hanyang.ac.kr (J.-H.L.); jbang@hanyang.ac.kr (J.H.B.).

Notes

The authors declare no competing financial interest.

■ ACKNOWLEDGMENTS

This work was supported by the Pioneer Research Center Program through the National Research Foundation of Korea (NRF, 2011-0001646) and by an NRF grant (2011-0028604) funded by the Ministry of Education, Science, and Technology (MEST). This work was also supported by the Human Resources Development of the Korea Institute of Energy Technology Evaluation and Planning (KETEP) grant funded by the Ministry of Knowledge Economy, Republic of Korea (20124030200130).

■ REFERENCES

(1) Kamat, P. V. *J. Phys. Chem. C* **2008**, *112*, 18737−18753.
(2) Rühle, S.; Shalom, M.; Zaban, A. *ChemPhysChem.* **2010**, *11*, 2290−2304.
(3) González-Pedro, V.; Xu, X. Q.; Mora-Seró, I.; Bisquert, J. *ACS Nano* **2010**, *4*, 5783−5790.
(4) Kamat, P. V. *Acc. Chem. Res.* **2012**, DOI: 10.1021/ar200315d.
(5) Lee, H. J.; Wang, M.; Chen, P.; Gamelin, D. R.; Zakeeruddin, S. M.; Grätzel, M.; Nazeeruddin, M. K. *Nano Lett.* **2009**, *9*, 4221−4227.
(6) Bang, J. H.; Kamat, P. V. *ACS Nano* **2011**, *5*, 9421−9427.
(7) Lee, Y. L.; Lo, Y. S. *Adv. Funct. Mater.* **2009**, *19*, 604−609.
(8) Guo, W.; Shen, Y. H.; Wu, M. X.; Ma, T. L. *Chem. Commun.* **2012**, *48*, 6133−6135.
(9) Itzhaik, Y.; Niitsoo, O.; Page, M.; Hodes, G. *J. Phys. Chem. C* **2009**, *113*, 4254−4256.
(10) Lee, H. J.; Chen, P.; Moon, S. J.; Sauvage, F.; Sivula, K.; Bessho, T.; Gamelin, D. R.; Comte, P.; Zakeeruddin, S. M.; Seok, S. I.; Grätzel, M.; Nazeeruddin, M. K. *Langmuir* **2009**, *25*, 7602−7608.
(11) Diguna, L. J.; Shen, Q.; Kobayashi, J.; Toyoda, T. *Appl. Phys. Lett.* **2007**, *91*, 023116.
(12) Tisdale, W. A.; Williams, K. J.; Timp, B. A.; Norris, D. J.; Aydil, E. S.; Zhu, X. Y. *Science* **2010**, *328*, 1543−1547.
(13) Nozik, A. J. *Inorg. Chem.* **2005**, *44*, 6893−6899.
(14) Chakrapani, V.; Baker, D.; Kamat, P. V. *J. Am. Chem. Soc.* **2011**, *133*, 9607−9615.
(15) Loucka, T. *J. Electroanal. Chem.* **1972**, *36*, 355−367.
(16) Giménez, S.; Mora-Seró, I.; Macor, L.; Guijarro, N.; Lana-Villarreal, T.; Gómez, R.; Diguna, L. J.; Shen, Q.; Toyoda, T.; Bisquert, J. *Nanotechnology* **2009**, *20*, 295204.
(17) Shi, J. F.; Fan, Y.; Xu, X. Q.; Xu, G.; Chen, L. H. *Acta Phys.−Chim. Sin.* **2012**, *28*, 857−864.
(18) Yang, Z.; Chen, C. Y.; Liu, C. W.; Chang, H. T. *Chem. Commun.* **2010**, *46*, 5485−5487.
(19) Tachan, Z.; Shalom, M.; Hod, I.; Rühle, S.; Tirosh, S.; Zaban, A. *J. Phys. Chem. C* **2011**, *115*, 6162−6166.
(20) Radich, J. G.; Dwyer, R.; Kamat, P. V. *J. Phys. Chem. Lett.* **2011**, *2*, 2453−2460.
(21) Paul, G. S.; Kim, J. H.; Kim, M. S.; Do, K.; Ko, J.; Yu, J. S. *ACS Appl. Mater. Interfaces* **2012**, *4*, 375−381.
(22) Dong, J. H.; Jia, S.; Chen, J. Z.; Li, B.; Zheng, J. F.; Zhao, J. H.; Wang, Z. J.; Zhu, Z. P. *J. Mater. Chem.* **2012**, *22*, 9745−9750.
(23) Riha, S. C.; Fredrick, S. J.; Sambur, J. B.; Liu, Y. J.; Prieto, A. L.; Parkinson, B. A. *ACS Appl. Mater. Interfaces* **2011**, *3*, 58−66.
(24) Riha, S. C.; Parkinson, B. A.; Prieto, A. L. *J. Am. Chem. Soc.* **2011**, *133*, 15272−15275.
(25) Guo, Q. J.; Hillhouse, H. W.; Agrawal, R. *J. Am. Chem. Soc.* **2009**, *131*, 11672−11673.
(26) Guo, Q. J.; Ford, G. M.; Yang, W. C.; Walker, B. C.; Stach, E. A.; Hillhouse, H. W.; Agrawal, R. *J. Am. Chem. Soc.* **2010**, *132*, 17384−17386.
(27) Shin, B.; Gunawan, O.; Zhu, Y.; Bojarczuk, N. A.; Chey, S. J.; Guha, S. *Prog. Photovolt: Res. Appl.* **2011**, DOI: 10.1002/pip.1174.
(28) Todorov, T. K.; Tang, J.; Bag, S.; Gunawan, O.; Gokmen, T.; Zhu, Y.; Mitzi, D. B. *Adv. Energy Mater.* **2012**, DOI: 10.1002/aenm.201200348.
(29) Xin, X. K.; He, M.; Han, W.; Jung, J.; Lin, Z. Q. *Angew. Chem., Int. Ed.* **2011**, *50*, 11739−11742.
(30) Ramasamy, K.; Malik, M. A.; O'Brien, P. *Chem. Sci.* **2011**, *2*, 1170−1172.
(31) Chen, S. Y.; Gong, X. G.; Walsh, A.; Wei, S. H. *Appl. Phys. Lett.* **2009**, *94*, 041903.
(32) Mitzi, D. B.; Gunawan, O.; Todorov, T. K.; Wang, K.; Guha, S. *Sol. Energy Mater. Sol. Cells* **2011**, *95*, 1421−1436.
(33) Schorr, S. *Sol. Energy Mater. Sol. Cells* **2011**, *95*, 1482−1488.
(34) Fan, S. Q.; Fang, B.; Kim, J. H.; Jeong, B.; Kim, C.; Yu, J. S.; Ko, J. *Langmuir* **2010**, *26*, 13644−13649.
(35) Wu, M. X.; Lin, X.; Wang, T. H.; Qiu, J. S.; Ma, T. L. *Energy Environ. Sci.* **2011**, *4*, 2308−2315.